Published in final edited form as:
J Control Release. 2011 February 28; 150(1): 37–44. doi:10.1016/j.jconrel.2010.10.025.

Optimizing Endothelial Targeting by Modulating the Antibody Density and Particle Concentration of Anti-ICAM Coated Carriers

Andres Calderon[1], **Tridib Bhowmick**[4], **John Leferovich**[2], **Bahrat Burmann**[1], **Benjamin Pichette**[1], **Vladimir Muzykantov**[2,3], **David Eckmann**[1,*], and **Silvia Muro**[4,5,*]

[1] Department of Anesthesiology and Critical Care, University of Pennsylvania Medical School, Philadelphia, PA, USA

[2] Institute for Environmental Medicine, University of Pennsylvania Medical School, Philadelphia, PA, USA

[3] Department of Pharmacology, University of Pennsylvania Medical School, Philadelphia, PA, USA

[4] Institute for Bioscience and Biotechnology Research, University of Maryland, College Park, MD, USA

[5] Fischell Department of Bioengineering, University of Maryland, College Park, MD, USA

Abstract

Targeting of drug carriers to cell adhesion molecules expressed on endothelial cells (ECs) may improve treatment of diseases involving the vascular endothelium. This is the case for carriers targeted to intercellular adhesion molecule 1 (ICAM-1), an endothelial surface protein overexpressed in many pathologies. In order to optimize our design of anti-ICAM carriers, we have explored in this study the influence of two carrier design parameters on specific and efficient endothelial targeting *in vitro* and *in vivo*: carrier dose and density of targeting molecules (antibodies -Ab-) on the carrier surface. Using radioisotope tracing we assessed the role of these parameters on the biodistribution of model polymer carriers targeted to ICAM-1 (^{125}I-anti-ICAM carriers) in mice. Increasing the carrier dose enhanced specific accumulation in the lung vasculature (a preferential endothelial target) and decreased non-specific hepatic and splenic uptake. Increasing the Ab density enhanced lung accumulation with minimally reduced liver and spleen uptake. These studies account for the influence of blood hydrodynamic forces on carrier binding to endothelium, relevant to arterioles, venules and larger vessels. Yet, carriers may rather bind to the extensive capillary bed where shear stress is minimal. We used fluorescence microscopy to determine binding kinetics of FITC-labeled anti-ICAM carriers in static conditions, at the threshold found *in vivo* and conditions mimicking low vs high ICAM-1 expression on quiescent vs activated ECs. Binding to activated ECs reached similar saturation with all tested Ab densities and carrier concentrations. In quiescent cells, carriers reached ~3-fold lower binding saturation, even at high carrier concentration and Ab density, and carriers with low Ab density did not reach saturation, reflecting avidity below threshold. Binding kinetics was positively regulated by anti-ICAM carrier concentration and Ab density. Counterintuitively, binding was faster in quiescent ECs (except for carriers with high Ab density and concentration), likely due to fast saturation of fewer binding sites on these cells. These results will guide optimization of ICAM-1-

[*]Correspondence should be addressed to: Silvia Muro (targeting to endothelial adhesion molecules): Institute for Bioscience and Biotechnology Research, 5115 Plant Sciences Building, College Park, MD 20742-4450, Tel. 1+301-405-4777, Fax. 1+301-314-9075, muro@umd.edu. David Eckmann (parameters of nanocarrier avidity): University of Pennsylvania, 331 John Morgan Building/6112, 3620 Hamilton Walk, Philadelphia, PA 19104-4215, USA, Tel. 1+215-349-5348, Fax. 1+215-349-5078, eckmanndm@uphs.upenn.edu.

targeted carriers, e.g., in the context of targeting healthy vs diseased endothelium for prophylactic vs therapeutic interventions.

Keywords

targeted drug carriers; endothelium; endothelial cell; ICAM-1; carrier concentration; antibody surface density; optimization

INTRODUCTION

An arsenal of carriers including liposomes, microbubbles, dendrimers, polimersomes, polymer particles, etc, is being developed for diagnostic and therapeutic applications [1–9]. Coupling of these carriers to antibodies (Abs) or other affinity moieties provides specific targeting to molecules expressed on the surface of the cells requiring intervention, enhancing the therapeutic effect [4,10–16]. The ability of a targeted carrier to reach a specific tissue depends on biological parameters and parameters inherent to the carrier design. Biological parameters include the shear stress that carriers need to withstand to remain bound to ECs in the circulation, and accessibility and level of expression of the target molecule, which also depend on the general and local pathophysiological status [17–23]. Carrier design features include their chemistry, size and shape, avidity and multivalency of targeting, carrier bulk concentration, etc. [5,17,24–27]. Defining these parameters is key to design carriers with optimal targeting properties.

Polymer carriers targeted to intercellular adhesion molecule 1 (ICAM-1) are a valuable model for this endeavor and hold translational relevance. ICAM-1, a transmembrane protein expressed primarily on endothelial cells (ECs) [28,29], is accessible to carriers injected in the circulation [18,25]. ICAM-1 is constitutively expressed on quiescent ECs and overexpressed on cells activated by many pathologies [28,29], providing targeting in prophylactic and therapeutic settings [4,12,19,20,30]. Carriers targeted to ICAM-1 by Abs (anti-ICAM carriers) bind specifically to ECs in culture and *in vivo* [11,18,22,25,26,31–39], showing good efficiency in a variety of applications [11,18,19,25,31,37,38].

We have previously studied the impact of design parameters and physiological conditions on the targeting of anti-ICAM carriers with different (i) composition (polystyrene vs poly(lactic-co-glycolic acid) or PLGA), [26], (ii) size and shape (0.1–10 μm, spherical vs elliptical disks) [25], and (iii) under different shear stresses (1 and 5 dyne/cm^2) [17]. Our results indicated: (i) similar performance of anti-ICAM polystyrene carriers vs PLGA carriers [26], (ii) higher specificity and efficacy of submicrometer spherical carriers and micrometer-range elongated carriers over other carrier geometries [25], and (iii) efficient EC targeting at 1 dyne/cm^2 shear stress, representative of small arterioles and venules [17].

To complete the identification of design parameters that are key to produce optimized ICAM-1-driven endothelial targeting, we have used radioisotope tracing and fluorescence microscopy of model anti-ICAM polystyrene carriers. We have explored *in vivo* and *in vitro* the role of: (i) density of the targeting Ab on the carrier surface impacting overall carrier avidity, and (ii) carrier bulk concentration. The results allow us to estimate more optimal design parameters of anti-ICAM carriers for healthy vs diseased endothelium. This is highly relevant for the development of more adequate prophylactic and therapeutic interventions using ICAM-1 targeting strategies.

MATERIALS AND METHODS

Antibodies and reagents

The monoclonal antibodies against human and mouse ICAM-1 were R6.5 [40] and YN1 [41]. Green fluorescent 1 μm and 0.1 μm diameter polystyrene particles were from Polysciences (Warrington, PA), $Na^{125}I$ was from Perkin Elmer (Wellesley, MA), and Iodogen was from Pierce Biotechnology (Rockford, IL). Other reagents were from Sigma Chemical (St. Louis, MO).

Preparation of anti-ICAM carriers

Anti-ICAM carriers and control IgG carriers were prepared by adsorption of anti-ICAM or non-specific IgG on the surface of polystyrene particles, as described [42,43]. Particles were centrifuged at 12,000 g for 5 min to separate Abs in solution from the surface-absorbed fraction [42,43]. To determine the amount of Ab coated on the particle surface, carriers were prepared by mixing anti-ICAM and ^{125}I-anti-ICAM at 90:10 molar ratio, as described [26]. For *in vivo* experiments, carriers contained a mixture of anti-ICAM and non-specific ^{125}I-IgG at 99:1, 99:5, 75:25, 25:75 or 0:100 molar ratio. The total amount of Abs coated per particle (including anti-ICAM and IgG) was kept constant to avoid variability due to different surface coatings [26]. Carriers where diluted in phosphate buffer saline with 3% bovine serum albumin and ultrasound sonicated [26]. This protocol avoids aggregation, confirmed by lack of carrier precipitation over a period of 48 h and by particle size measured by dynamic light scattering. The diameter of the coated carriers averaged 0.179 ± 0.038 μm and 1.14 ± 0.21 μm, respectively, with a z-potential ~−20mV [25,26]. A description of all different parameters concerning the carriers used in this work is provided in Tables 1 and 2.

Targeting of anti-ICAM carriers in mice

For these experiments we selected submicrometer carriers, a size that precludes from non-specific entrapment in capillaries and more amenable for future translational applications. Control male C57BL/6 mice or mice pre-treated intraperitonealy for 16 h with bacterial lipopolysaccharide (LPS), were anesthetized and injected intravenously with saline solutions containing different amounts of ^{125}I-labeled anti-ICAM carriers (2.3×10^{10}, 23×10^{10} or 65×10^{10} carrier particles/ml of blood; 7.2×10^{8}, 72.2×10^{8}, 204.1×10^{8} μm^2 carrier-surface/ml of blood), or carriers with different Ab densities on their surface (from 1750 to 6,935 Ab/μm^2), hence presenting from 48×10^{11} to $1,357 \times 10^{11}$ Ab/ml of blood. Carriers with only IgG and no anti-ICAM were controls.

Blood and organ samples were collected 30 min after injection: lungs that are a specific target organ for endothelial-addressed carriers vs liver and spleen that nonspecifically clear carriers and Fc-containing Abs [25,26]. The samples' radioactivity and weight were determined to calculate carrier circulation as percent of injected dose (%ID) in blood, and carrier biodistribution as %ID per gram of organ (%ID/g) that allows to compare between organs of different weight. These studies followed the Guide for the Care and Use of Laboratory Animals adopted by the National Institutes of Health, and were approved by the University of Maryland's and University of Pennsylvania's IACUC committees.

Cell culture

Human umbilical vein ECs (HUVECs) (Lonza, San Diego, CA) were cultured on gelatin-coated glass coverslips [43]. Cells were incubated at 37°C, 5% CO_2 and 95% humidity in M199 medium supplemented as described [43]. To mimic activation of ECs causing maximal expression of ICAM-1, cells were treated overnight with 10 ng/mL of TNF-α vs. control media used for resting or quiescent ECs expressing minimal levels of ICAM-1.

Previous work has shown ~20–100 fold increased ICAM-1 expression in activated over quiescent cells (maximal expression ~10^6 molecules/activated cell) [11,19,26]. Cells fixed with 2% paraformaldehyde prior to experiments were used instead of live cells to avoid the confounding influence of concomitant carrier internalization by cells [43]. We have verified that binding is similar in fixed and live cells during the first 15 min of incubation [17], validating this model. Of note, internalization of anti-ICAM carriers within ECs has been shown to provide an interesting avenue for intraendothelial drug delivery both *in vitro* and *in vivo* [11,26,35].

Carrier binding in cell culture

For accurate imaging, 1 μm carriers were used in these experiments, yet their formulation was adjusted to obtain values of total carrier surface in the cell medium (μm^2/ml) and total targeting Abs in the cell medium (Ab/μm^2 and Ab/ml) similar to some of those used for 0.1 μm carriers injected in mice. Resting or activated ECs were incubated from 2 min to 24 h with anti-ICAM carriers vs control IgG carriers at two different carrier concentrations: 6.8×10^8 vs 13×10^8 carriers/ml (21×10^8 vs 41×10^8 μm^2 carrier-surface/ml), each of them displaying two Ab surface densities: 1,100 Ab/μm^2 vs 4,100 Ab/μm^2 (hence, from 23.4×10^{11} to 167.4×10^{11} Ab/ml) (Table 2). Unbound carriers were washed and the samples were analyzed in a fluorescence microscope (Eclipse TE2000-U; Nikon, Melville, NY) with a 40x/NA1.4 PlanApo objective (Nikon). The number of fluorescent carriers bound per cell at each time point was determined from micrographs obtained with an Orca-1 CCD camera (Hamamatsu; Bridgewater, NJ) using ImagePro 3.0 (Media Cybernetics, Silver Spring, MD). The results were used to determine the experimental and theoretical halftimes of carrier binding ($t_{1/2}$ and K_t) and to estimate their maximum saturating binding (B_{sat}) using SigmaPlot (Systat Software, Inc.; San Jose, CA).

In addition, the avidity of anti-ICAM carriers toward ECs was estimated at 1 h using carrier concentrations between 1.1×10^8 and 68×10^8 carriers/ml. The effective K_d and B_{max} were determined from the Scatchard curves using non-linear regression and Sigma Plot software.

Statistics

Data were calculated as mean ± standard error of the mean. Statistical significance, determined by Student's t test, as considered to be reached for $p < 0.05$.

RESULTS AND DISCUSSION

Endothelial targeting of anti-ICAM carriers in mice: effects of Ab density on the carrier surface

Previous studies have shown preferential accumulation of anti-ICAM carriers in lung [25,26,35], an organ that has a high level of ICAM-1 constitutive expression, receives the entirety of the cardiac output (i.e., 100% of the venous blood) and contains a marked fraction of the endothelial surface in the body [4,18,44]. Anti-ICAM carriers also undergo relatively unspecific clearance by the liver and spleen [25,26,35], a phenomena observed for objects which exceed the filtration limit of the kidney and coated with Abs containing Fc fragments amenable for binding to Fc receptors in macrophages in these organs. Therefore, we explored the influence of parameters such as the carrier concentration and antibody surface density in accumulation of anti-ICAM carriers in lung vs liver and spleen (Table 1).

Using radioisotope tracing and confirming previous results, anti-ICAM carriers bearing 6,935 Ab/μm^2 (carrier surface saturated with Ab) rapidly disappeared from the circulation (< 4.6 ± 0.7 percent injected dose -%ID- by 30 min) (Figure 1A) and specifically accumulated in the lung vasculature (125.0 ± 16.8 percent injected dose per gram of organ, %ID/g) vs

control IgG carriers (9.3 ± 1.4 %ID/g, marked as 0 Ab/μm^2) (Figure 1B). Compared to lung, anti-ICAM carriers accumulated at a much lower extent in the liver and spleen (45.0 ± 6.2 %ID/g and 65.4 ± 7.0 % ID/g, respectively) with increasing anti-ICAM density (Figure 1B). Lung accumulation of carriers was correlated positively with the density of anti-ICAM molecules on the carrier surface: reduction of 5%, 25% and 75% in the Ab surface density resulted in 20%, 50%, and 60% reductions in the pulmonary accumulation of carriers. Yet, at low anti-ICAM surface density, considerable lung targeting still occurred (Figure 1B). These reductions in the Ab surface density led to modest increases in the accumulation of anti-ICAM carriers in the liver (0%, 3%, and 6% increases) and spleen (0%, 2%, and 10%). All carriers disappeared from the circulation similarly (Figure 1A), suggesting that lung targeting occurs similarly faster than clearance by the liver and spleen.

At low anti-ICAM surface density, carrier accumulation per gram of spleen surpassed that of the liver, while increasing anti-ICAM surface density equalized carrier accumulation in these organs (Figure 1B). Hence, surface density effects had a greater impact on uptake by the spleen. This correlates well with the smaller size of the spleen (~10 fold lesser weight than liver), for which an increased accumulation reflects a greater change as expressed by organ weight. Uptake by the profuse monocyte-macrophage system present in the spleen (mediated by Fc-mediated uptake and phagocytosis of particles) may also contribute to enhance the accumulation of low Ab-surface density anti-ICAM carriers in this organ. In any case, increasing the Ab-surface density is a simple approach for improving carrier delivery to specific organs, such as the lung in the case of anti-ICAM carriers, while reducing non-specific uptake by “filtering” systems in the liver and spleen. Although this seems predictable, one must consider that ICAM-1 is also expressed by cells in these organs, e.g., the liver expresses 130% of lung ICAM-1 levels normalized to total protein [18]. Predominant accumulation of anti-ICAM carriers in the lung vasculature may be due to a first-pass effect, in accord with fast disappearance of carriers for the blood and fast binding *in vivo*. Injection routes avoiding the lung as a first-pass organ (e.g., intra-arterial injections other than in pulmonary arteries) may shift anti-ICAM carrier uptake to other organs.

Surprisingly, carriers with only 25% surface covered by anti-ICAM had marked and specific lung uptake vs IgG carriers (55.8 ± 6.7 %ID/g vs 9.3 ± 1.4 %ID/g). A significant fraction of the carrier surface may be used for coupling of other targeting moieties, membrane penetrating agents, cargoes, or imaging molecules. Indeed, previous works showed EC targeting by anti-ICAM carriers with enzymes on their surface (anti-oxidant catalase or acid sphingomyelinase for lysosomal therapy) [11,18,25,26].

Endothelial targeting of anti-ICAM carriers in mice: effects of the carrier concentration

The assays described refer to 23×10^{10} carrier particles/ml blood. To test the effect of carrier concentration *in vivo* we compared this concentration to ~0.1 and ~3 fold variations (carriers = 6,650 Ab/μm^2).

Regardless of the concentration of particles, anti-ICAM carriers disappeared rapidly from the circulation (Figure 2A). Even at the maximal concentration, anti-ICAM carriers accumulated in lung with high specificity (10 fold above IgG carriers, Figure 2A and Supplementary Figure 1), ruling out mechanical entrapment. Uptake in the lung decreased with reduced carrier concentrations, yet it was still relevant: reduction of the anti-ICAM carrier concentration by 65% or 97% led to 45% and 60% reductions in lung accumulation, respectively (Figure 2B). In parallel, 23% and 100% increases in carrier uptake in the liver and 20% and 45% increases in the spleen were observed (statistical significance was reached only for the liver).

The absolute amount of carriers cleared by the liver and spleen increased with the carrier dose, suggesting that clearing capacity was not saturated. Comparison of all anti-ICAM carrier formulations (in which carrier dose or Ab surface density were varied) showed that increased specific accumulation in the lung and reduction in non-specific uptake by the liver and spleen correlated positively with the blood concentration of the injected carrier-bound antibody (Table 3). This correlation appeared linear (intercept, 34 %ID/g of lung; slope, 1.2×10^{-12}, $r^2 = 0.89$) suggesting that saturation was not reached.

In contrast to modification of the Ab surface density on carriers, the dose of particles had a greater impact on uptake by the liver than by the spleen, likely due to the smaller spleenic clearance capacity, given the greater amount of carriers diverging from the lung to clearing organs. Increasing the concentration of anti-ICAM carriers had a greater impact on the non-specific uptake in the liver and spleen than varying the Ab surface density on carriers. This suggests that modifying the carrier concentration (within a given interval) may enhance specificity of targeting to organs, such as the lung for anti-ICAM carriers, vs non-specific clearance by the liver and spleen. This is relevant in limiting delivery of therapeutics to non-intended destinations minimize potential toxicity and side effects.

Endothelial targeting of anti-ICAM carriers in mice: effects of the endothelial phenotype

Using an intermediate parameter of carrier concentration and Ab surface density (23×10^{10} carrier particles/ml blood and 6,650 Ab/μm^2) we compared the biodistribution of anti-ICAM carriers in control mice vs mice challenged by LPS to mimic inflammation, known to increase ICAM-1 expression (Materials & Methods and [19]). LPS led to increased carrier accumulation in the lung vasculature (148 ± 12.9 % of control mice) with no changes in the hepatic and splenic clearance (103.6 ± 9.1 and 106.5 ± 29.8 % of control mice) (Figure 3). This is in accord with prior works demonstrating enhanced ICAM-1 targeting to areas affected by inflammation [45] and emphasizes the relevance of biological target expression parameters on carrier binding *in vivo*.

Kinetics of endothelial targeting of anti-ICAM carriers in cell culture: effects of Ab density on the carrier

Data from *in vivo* experiments illustrate the relevance of the parameters studied and suggest that low concentration of carriers or low levels of Ab on the carrier surface still render endothelial targeting. This may be, at least in part, due to primary binding of anti-ICAM carriers in capillaries, where the shear stress in negligible. Using fluorescence microscopy and static cell culture, we explored the kinetics of binding of anti-ICAM carriers in an interval of parameters around the Ab threshold for specific binding (Table 2): 21×10^8 and 41×10^8 μm^2 carrier-surface/ml (i.e., 1,100 and 4,100 Ab/μm^2 or ~ 2.3×10^{12} and 17×10^{12} Ab/ml). Binding was also tested as a function of the cell status: in quiescent ECs that express a basal level of ICAM-1, like in healthy endothelium [19,46], vs TNF-α activated cells which overexpress ICAM-1 and mimic pathologically altered endothelium [19,26,46].

Supplementary Figure 2 shows microscopy images of anti-ICAM carriers binding to ECs as a function of time and Ab surface density, also demonstrating lack of specific binding of IgG carriers. The experimental halftime of binding ($t_{1/2}$) and maximal binding at saturation (B_{sat}) were determined by image analysis, while the theoretical halftime (K_t) was estimated by non-linear regression (Table 4).

We compared the binding kinetics of carriers coated by Ab at different surface densities (1,100 or 4,100 Ab/μm^2) and low carrier dose (equivalent to a surface area density 21.3×10^8 μm^2/ml) in quiescent ECs. The binding kinetics (Figure 4 and Table 4) was faster for carriers with high Ab surface density ($t_{1/2}$ = 60 min vs 250 min for low Ab-density carriers,

$p < 0.05$). Carriers reached different maximal binding levels: 52 ± 8 vs 16 ± 3 carriers/cell for higher and lower Ab-density carriers. Binding of low Ab-density anti-ICAM carriers was comparable to that of IgG carriers (11 ± 2 carriers/cell), in opposition to *in vivo* results. Yet, the formulations selected for *in vitro* assays were in the threshold of specific/effective binding observed *in vivo*. Also, quiescent ECs *in vivo* express high ICAM-1 levels vs low levels in quiescent cultures [19]. In addition, the maximum binding level of anti-ICAM carriers bearing 4,100 Ab/μm^2 to quiescent cells was only 2 fold greater than IgG carriers (Figure 4), implying that this may be a threshold value of Ab surface density in these cells. This is equivalent to 58×10^{11} Ab/ml, similar to the level of Ab concentration provided by anti-ICAM carriers found to specifically bind to the lung endothelium in control mice (48×10^{11} Ab/ml, Table 3).

We then compared the binding kinetics of these carriers in activated ECs (Figure 5 and Table 4), which was faster for carriers with high Ab surface density ($t_{1/2}$ = 120 min vs 300 min for low Ab-density carriers, $p < 0.05$). In contrast to resting ECs, the binding kinetics of low Ab-density carriers differed from that of IgG carriers ($p < 0.01$). This behavior is similar to that of receptor-ligand pairing where a minimal receptor density threshold must be exceeded in order for a ligand to bind linearly to the receptor [47]. Although anti-ICAM carriers with low Ab-surface density do not target ICAM-1 on quiescent ECs they do target activated ECs. This may reduce endothelial binding in healthy regions of the body despite basal ICAM-1 expression, while providing targeting to disease sites high ICAM-1 expression.

In contrast, in activated ECs the binding of anti-ICAM carriers with low or high Ab-surface density reached a similar maximal level: 165 ± 10 vs 171 ± 14 carriers/cell. This accounts for ~ 80% of the total cell surface area [17], hence, carriers bind to all accessible ICAM-1. Low Ab-surface density carriers reach similar levels of binding in activated ECs and display specific binding at any given time point vs IgG carriers. As observed *in vivo* (Figure 1 and Table 3), this suggests that the carrier surface can be shared by cargoes without markedly compromising targeting properties of anti-ICAM carriers.

As expected, the number of anti-ICAM coated carriers bound per cell at any given time and the maximal binding at saturation was higher in activated vs quiescent cells, for both Ab surface densities (Table 4). This is in accord with up-regulated ICAM-1 expression in activated ECs [19,46] and correlates well with results *in vivo* (Figure 3). The binding kinetics of either type of carrier (low vs high Ab-surface density) was faster for quiescent vs activated cells (Table 4). This may seem counterintuitive, given that one would expect that higher ICAM-1 expression would contribute to a higher avidity of anti-ICAM carriers. Yet, the earlier saturation of fewer ICAM-1 receptors available for binding anti-ICAM carriers can explain a faster kinetics.

Kinetics of endothelial targeting of anti-ICAM carriers in cell culture: effects of the carrier concentration

We then evaluated anti-ICAM carriers displaying 1,100 Ab/μm^2 in quiescent and activated ECs at two different concentrations: 6.8×10^8 vs 13×10^8 carriers/ml, equivalent to 21×10^8 vs 41×10^8 μm^2 carrier-surface/ml (Figure 6 and Table 4). At high carrier concentrations, the binding kinetics of anti-ICAM carriers was faster for quiescent vs activated cells ($t_{1/2}$ = 30 min vs 180 min), and maximal binding was also positively correlated with EC activation (35 vs 173 carriers/cell). This pattern is similar to that of carriers incubated at a low concentration with cells and *in vivo* (Figures 2B and 3). However, whereas low Ab-density carriers did not show specific binding (over IgG carriers) to quiescent cells when applied at a low concentration (6.8×10^8 carriers/ml), at a higher concentration (13×10^8 carriers/ml) the same carriers displayed specific binding (e.g., 35

carriers/cell vs 11 carriers/cell for IgG carriers). Therefore, simply modifying the concentration of the anti-ICAM carrier dose without affecting the carrier formulation, the binding selectivity can be shifted toward quiescent endothelium.

For both quiescent and activated cells, increasing carrier concentration accelerated the binding kinetics: from 250 min to 30 min in quiescent cells and from 300 min to 180 min in activated cells. However, increasing the carrier concentration only enhanced the maximal level of binding at saturation in quiescent cells (from 16 to 35 carriers/cell). In activated cells, increasing the carrier concentration did not enhance maximal binding (173 ± 11 vs 165 ± 10 carriers/cell). This suggests saturation of ICAM-1 molecules accessible for molecular targeting and the cellular surface available for carrier binding.

We also examined *in vitro* effects of modifying the carrier concentration in the case of anti-ICAM carriers with high Ab-surface density (4,100 Ab/μm^2; Figure 7 and Table 4). In quiescent ECs, increasing the concentration of anti-ICAM carriers did not increase the binding kinetics ($t_{1/2}$ = 60 min) or maximal binding at saturation (58 ±9 and 52 ± 8 carriers/cell). This suggests that the avidity of anti-ICAM carriers with 4,100 Ab/μm^2 may be above the threshold of ICAM-1 expression in quiescent cells. Increasing the carrier concentration did not increase the binding kinetics. Manipulation of the carrier concentration to improve endothelial targeting becomes less relevant for carriers with high Ab-density in the context of prophylactic interventions due to low ICAM-1 expression. In contrast, in pathologically activated ECs, increasing the carrier concentration accelerates the binding kinetics from 120 min to 60 min (Figure 7 and Table 4). This suggests a greater sensitivity to modulation of the dose of anti-ICAM carriers, important in optimizing targeting to diseased sites. These data correlates with the enhanced targeting of anti-ICAM carriers to lungs in LPS treated mice (which upregulates ICAM-1 expression, Figure 3), allowing us to adjust parameters to achieve optimized targeting to sites affected by disease.

Avidity of anti-ICAM carriers

In vitro and *in vivo* results suggest an increasing avidity of anti-ICAM carriers bearing low vs high density of targeting Abs on the surface, and also in the case of high ICAM-1 expression on target cells. To verify this, we determined the avidity of carriers used *in vitro* (1,100 vs 4,100 Ab/μm^2) toward either quiescent or activated ECs, using carrier concentrations varying from 1.1×10^8 to 68×10^8 carriers/ml and calculating the K_d and B_{max} values using Scatchard analysis (Table 5).

Confirming this, the avidity of anti-ICAM carriers increased with increasing Ab density: 2.9 pM vs 1.6 pM for 1,100 vs 4,100 Ab/μm^2 carriers. In addition, increased ICAM-1 expression in activated cells led to increased avidity of anti-ICAM carriers: 5.9 pM to 1.6 pM for 4,100 Ab/μm^2 carriers.

Regarding maximal binding, both low and high Ab-surface density carriers reached similar levels in activated cells, likely due to saturation of the ICAM-1 binding sites and/or cellular surface area available. Maximal binding increased with cell activation: from 55 to 175 carriers/cell for 4,100 Ab/μm^2 anti-ICAM carriers. Avidity data pair well with experimental findings and support our conclusions.

CONCLUSIONS

Understanding how design parameters such as carrier bulk concentration and Ab surface density affect the binding of drug carriers to the target cells is crucial to optimize their efficacy. One would expect that increasing the Ab surface density and concentration of carriers would result in an improved specificity, faster kinetics, and enhanced amount of

carriers reaching the target cells. Although this is the case for the most part, in this work focusing on carriers targeted to endothelial ICAM-1 we have shown that this correlation greatly depends on biological parameters such as the level of expression of the target molecule, which may vary between control and pathological conditions. Anti-ICAM carriers with apparent sub-optimal avidity may provide increased selectivity toward diseased areas where ICAM-1 is overexpressed vs anti-ICAM carriers with greater avidity. Although this paradigm holds less relevance in vascular areas subjected to significant shear stress (where carriers need to overcome important hydrodynamic forces) [17], it applies to vascular regions with negligible shear stress, e.g., the extensive capillary network where most carriers might bind, and likely ischemic areas known to express high levels of ICAM-1. Such a paradigm also allows for minimization of the amount of targeting Ab to be used (coating of only 25–50% of the carrier surface shows specific targeting), likely improving potential side effects and permitting coupling of cargoes on the remaining carrier surface without losing main targeting capabilities. In the case of drug delivery for prophylactic interventions, greater concentrations of low avidity anti-ICAM carriers can be used or concentration can be maintained by switching to high avidity carriers. These results have allowed us to identify particular anti-ICAM carrier designs valuable for prophylactic vs therapeutic interventions targeted to healthy vs diseased endothelium.

Supplementary Material

Refer to Web version on PubMed Central for supplementary material.

Acknowledgments

This work was funded by NIH T32 GM007612, R01 HL60230S1, and R01 EB006818 (DME), P01 HL079063 and R01 HL087036 (VM), and AHA 09BGI2450014, and R01 HL098416 (SM). We thank Dr. Carmen Garnacho and Dr. Shunji Kobayashi for technical assistance and Neeraj J. Agrawal and Dr. Ravi Radhakrishnan for their insightful discussion on quantitative approaches.

References

1. Discher DE, Eisenberg A. Polymer vesicles. Science. 2002; 297:967–973. [PubMed: 12169723]
2. Klibanov AL. Ligand-carrying gas-filled microbubbles: Ultrasound contrast agents for targeted molecular imaging. Bioconjug Chem. 2005; 16:9–17. [PubMed: 15656569]
3. Kabanov AV, Batrakova EV, Alakhov VY. Pluronic (R) block copolymers as novel polymer therapeutics for drug and gene delivery. J Controlled Release. 2002; 82:189–212.
4. Muzykantov VR. Biomedical aspects of targeted delivery of drugs to pulmonary endothelium. Expert Opin Drug Del. 2005; 2:909–926.
5. Dziubla TD, Muzykantov VR. Synthetic carriers for vascular delivery of protein therapeutics. Biotechnol Genet Eng Rev. 2006; 22:267–298. [PubMed: 18476335]
6. Davda J, Labhasetwar V. Characterization of nanoparticle uptake by endothelial cells. Int J Pharm. 2002; 233:51–59. [PubMed: 11897410]
7. Torchilin VP. Multifunctional and stimuli-sensitive pharmaceutical nanocarriers. Eur J Pharm Biopharm. 2009; 71:431–444. [PubMed: 18977297]
8. Batrakova EV, Kabanov AV. Pluronic block copolymers: Evolution of drug delivery concept from inert nanocarriers to biological response modifiers. J Controlled Release. 2008; 130:98–106.
9. Hoffman AS. The origins and evolution of “controlled” drug delivery systems. J Controlled Release. 2008; 132:153–163.
10. Shmeeda H, Tzernach D, Mak L, Gabizon A. Her2-targeted pegylated liposomal doxorubicin: Retention of target-specific binding and cytotoxicity after in vivo passage. J Controlled Release. 2009; 136:155–160.

11. Muro S, Schuchman EH, Muzykantov VR. Lysosomal enzyme delivery by ICAM-1-targeted nanocarriers bypassing glycosylation- and clathrin-dependent endocytosis. Mol Ther. 2006; 13:135–141. [PubMed: 16153895]
12. Muzykantov VR. Immunotargeting of drugs to the pulmonary vascular endothelium as a therapeutic strategy. Pathophysiology. 1998; 5:15–33.
13. Saad M, Garbuzenko OB, Ber E, Chandna P, Khandare JJ, Pozharov VP, Minko T. Receptor targeted polymers, dendrimers, liposomes: Which nanocarrier is the most efficient for tumor-specific treatment and imaging? J Controlled Release. 2008; 130:107–114.
14. Hossen N, Kajimoto K, Akita H, Hyodo M, Ishitsuka T, Harashima H. Ligand-based targeted delivery of a peptide modified nanocarrier to endothelial cells in adipose tissue. J Controlled Release. 201010.1016/j.jconrel.2010.07.100
15. Morse DL, Gillies RJ. Molecular imaging and targeted therapies. Biochem Pharmacol. 2010; 80:731–738. [PubMed: 20399197]
16. Molema G. Tumor vasculature directed drug targeting: applying new technologies and knowledge to the development of clinically relevant therapies. Pharm Res. 2002; 19:1251–1258. [PubMed: 12403059]
17. Calderon AJ, Muzykantov V, Muro S, Eckmann DM. Flow dynamics, binding and detachment of spherical carriers targeted to ICAM-1 on endothelial cells. Biorheology. 2009; 46:323–341. [PubMed: 19721193]
18. Garnacho C, Dhami R, Simone E, Dziubla T, Leferovich J, Schuchman EH, Muzykantov V, Muro S. Delivery of acid sphingomyelinase in normal and Niemann-Pick disease mice using intercellular adhesion molecule-1-targeted polymer nanocarriers. J Pharmacol Exp Ther. 2008; 325:400–408. [PubMed: 18287213]
19. Murciano JC, Muro S, Koniaris L, Christofidou-Solomidou M, Harshaw DW, Albelda SM, Granger DN, Cines DB, Muzykantov VR. ICAM-directed vascular immunotargeting of antithrombotic agents to the endothelial luminal surface. Blood. 2003; 101:3977–3984. [PubMed: 12531816]
20. Eniola AO, Hammer DA. Artificial polymeric cells for targeted drug delivery. J Controlled Release. 2003; 87:15–22.
21. Eniola AO, Willcox PJ, Hammer DA. Interplay between rolling and firm adhesion elucidated with a cell-free system engineered with two distinct receptor-ligand pairs. Biophys J. 2003; 85:2720–2731. [PubMed: 14507735]
22. Sakhalkar HS, Dalal MK, Salem AK, Ansari R, Fu J, Kiani MF, Kurjiaka DT, Hanes J, Shakesheff KM, Goetz DJ. Leukocyte-inspired biodegradable particles that selectively and avidly adhere to inflamed endothelium in vitro and in vivo. Proc Natl Acad Sci USA. 2003; 100:15895–15900. [PubMed: 14668435]
23. Doshi N, Prabhakarpandian B, Rea-Ramsey A, Pant K, Sundaram S, Mitragotri S. Flow and adhesion of drug carriers in blood vessels depend on their shape: A study using model synthetic microvascular networks. J Controlled Release. 2010; 146:196–200.
24. Dziubla TD, Shuvaev VV, Hong NK, Hawkins BJ, Madesh M, Takano H, Simone E, Nakada MT, Fisher A, Albelda SM, Muzykantov VR. Endothelial targeting of semi-permeable polymer nanocarriers for enzyme therapies. Biomaterials. 2008; 29:215–227. [PubMed: 17950837]
25. Muro S, Garnacho C, Champion JA, Leferovich J, Gajewski C, Schuchman EH, Mitragotri S, Muzykantov VR. Control of endothelial targeting and intracellular delivery of therapeutic enzymes by modulating the size and shape of ICAM-1-targeted carriers. Mol Ther. 2008; 16:1450–1458. [PubMed: 18560419]
26. Muro S, Dziubla T, Qiu W, Leferovich J, Cui X, Berk E, Muzykantov VR. Endothelial targeting of high-affinity multivalent polymer nanocarriers directed to intercellular adhesion molecule 1. J Pharmacol Exp Ther. 2006; 317:1161–1169. [PubMed: 16505161]
27. Decuzzi P, Ferrari M. Design maps for nanoparticles targeting the diseased microvasculature. Biomaterials. 2008; 29:377–384. [PubMed: 17936897]
28. Springer TA. Adhesion Receptors of the Immune-System. Nature. 1990; 346:425–434. [PubMed: 1974032]

29. Muro, S. Intercellular Adhesion Molecule-1 and Vascular Cell Adhesion Molecule-1. In: Aird, WC., editor. Endothelial Biomedicine. New York: Cambridge University Press; 2007. p. 1058-1070.

30. Muro S, Muzykantov VR. Targeting of antioxidant and anti-thrombotic drugs to endothelial cell adhesion molecules. Curr Pharm Des. 2005; 11:2383–2401. [PubMed: 16022673]

31. Bloemen PG, Henricks PA, van Bloois L, van den Tweel MC, Bloem AC, Nijkamp FP, Crommelin DJ, Storm G. Adhesion molecules: a new target for immunoliposome-mediated drug delivery. FEBS Lett. 1995; 357:140–144. [PubMed: 7805880]

32. Luo GX, Kohlstaedt LA, Charles CH, Gorfain E, Morantte I, Williams JH, Fang F. Humanization of an anti-ICAM-1 antibody with over 50-fold affinity and functional improvement. J Immunol Methods. 2003; 275:31–40. [PubMed: 12667668]

33. Kozower BD, Christofidou-Solomidou M, Sweitzer TD, Muro S, Buerk DG, Solomides CC, Albelda SM, Patterson GA, Muzykantov VR. Immunotargeting of catalase to the pulmonary endothelium alleviates oxidative stress and reduces acute lung transplantation injury. Nat Biotechnol. 2003; 21:392–398. [PubMed: 12652312]

34. Ding BS, Dziubla T, Shuvaev VV, Muro S, Muzykantov VR. Advanced drug delivery systems that target the vascular endothelium. Mol Interv. 2006; 6:98–112. [PubMed: 16565472]

35. Muro S, Gajewski C, Koval M, Muzykantov VR. ICAM-1 recycling in endothelial cells: a novel pathway for sustained intracellular delivery and prolonged effects of drugs. Blood. 2005; 105:650–658. [PubMed: 15367437]

36. Takei Y, Nishimura Y, Kawano S, Nagai H, Ohmae A, Fusamoto H, Kamada T. Expression of ICAM-1 is involved in the mechanism of liver injury during liver transplantation: therapeutic usefulness of the F(ab′)2 fragment of an anti-ICAM-1 monoclonal antibody. Transplant Proc. 1996; 28:1103–1105. [PubMed: 8623241]

37. Villanueva FS, Jankowski RJ, Klibanov S, Pina ML, Alber SM, Watkins SC, Brandenburger GH, Wagner WR. Microbubbles targeted to intercellular adhesion molecule-1 bind to activated coronary artery endothelial cells. Circulation. 1998; 98:1–5. [PubMed: 9665051]

38. Weiner RE, Sasso DE, Gionfriddo MA, Thrall RS, Syrbu S, Smilowitz HM, Vento J. Early detection of oleic acid-induced lung injury in rats using (111)In-labeled anti-rat intercellular adhesion molecule-1. J Nucl Med. 2001; 42:1109–1115. [PubMed: 11438635]

39. Weller GE, Villanueva FS, Klibanov AL, Wagner WR. Modulating targeted adhesion of an ultrasound contrast agent to dysfunctional endothelium. Ann Biomed Eng. 2002; 30:1012–1019. [PubMed: 12449762]

40. Marlin SD, Springer TA. Purified intercellular adhesion molecule-1 (ICAM-1) is a ligand for lymphocyte function-associated antigen 1 (LFA-1). Cell. 1987; 51:813–819. [PubMed: 3315233]

41. Jevnikar AM, Wuthrich RP, Takei F, Xu HW, Brennan DC, Glimcher LH, Rubin-Kelley VE. Differing regulation and function of ICAM-1 and class II antigens on renal tubular cells. Kidney Int. 1990; 38:417–425. [PubMed: 1977950]

42. Wiewrodt R, Thomas AP, Cipelletti L, Christofidou-Solomidou M, Weitz DA, Feinstein SI, Schaffer D, Albelda SM, Koval M, Muzykantov VR. Size-dependent intracellular immunotargeting of therapeutic cargoes into endothelial cells. Blood. 2002; 99:912–922. [PubMed: 11806994]

43. Muro S, Wiewrodt R, Thomas A, Koniaris L, Albelda SM, Muzykantov VR, Koval M. A novel endocytic pathway induced by clustering endothelial ICAM-1 or PECAM-1. J Cell Sci. 2003; 116:1599–1609. [PubMed: 12640043]

44. Murciano JC, Medinilla S, Eslin D, Atochina E, Cines DB, Muzykantov VR. Prophylactic fibrinolysis through selective dissolution of nascent clots by tPA-carrying erythrocytes. Nat Biotechnol. 2003; 21:891–896. [PubMed: 12845330]

45. Rossin R, Muro S, Welch MJ, Muzykantov VR, Schuster DP. In vivo imaging of Cu-64-labeled polymer nanoparticles targeted to the lung endothelium. J Nucl Med. 2008; 49:103–111. [PubMed: 18077519]

46. Remy M, Valli N, Brethes D, Labrugere C, Porte-Durrieu MC, Dobrova NB, Novikova SP, Gorodkov AJ, Bordenave L. In vitro and in situ intercellular adhesion molecule-1 (ICAM-1)

expression by endothelial cells lining a polyester fabric. Biomaterials. 1999; 20:241–251. [PubMed: 10030601]

47. Matsuoka T, Hardy C, Tavassoli M. Characterization of Membrane Homing Receptors in 2 Cloned Murine Hematopoietic Progenitor-Cell Lines. J Clin Invest. 1989; 83:904–911. [PubMed: 2493486]

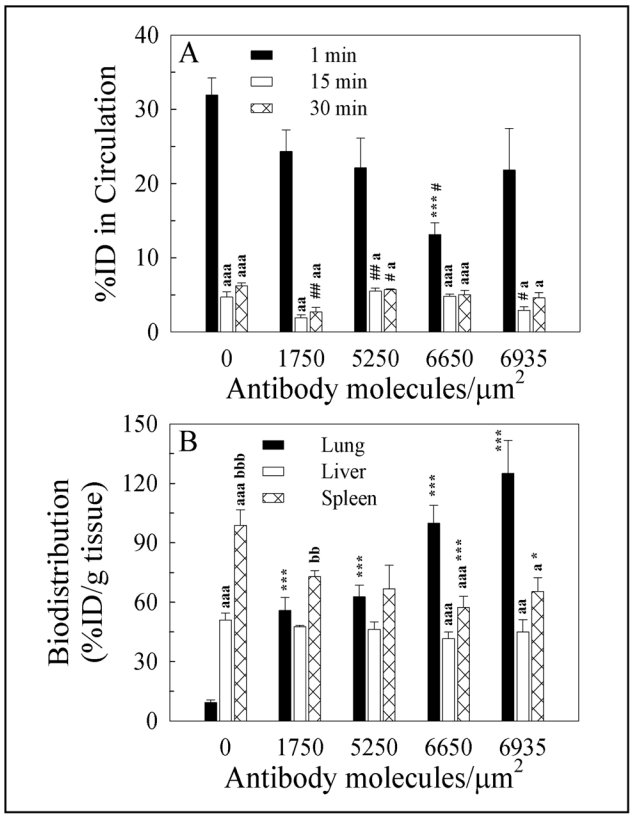

Figure 1. Effects of the Ab-surface density of anti-ICAM carriers on endothelial targeting in mice

(A) Circulation of ^{125}I-labeled anti-ICAM carriers (23×10^{10} carriers/ml blood) bearing varying Ab-surface densities (as indicated) at 1 min, 15 min, and 30 min after i.v. injection in anesthetized C57Bl/6 mice, expressed as the percentage of the injected dose (%ID). (B) Biodistribution of said carriers at 30 min after injection, calculated as % ID per gram of organ. Data are mean ± SEM (n ≥ 3 mice). Control IgG carriers are represented as 0 Ab/μm^2. Among different groups of carriers: * compares each Ab-surface density carrier to carriers with Ab surface density = 0; # compares each Ab-surface density carrier to the immediate lower Ab-surface density carrier. Within the same group of carrier: a compares each time to 1 min; b compares 30 min to 15 min. *, #, a, and b are $p \leq 0.05$; **, ##, aa, and bb are $p \leq 0.01$; ***, ###, aaa, and bbb are $p \leq 0.001$, by Student's *t*-test.

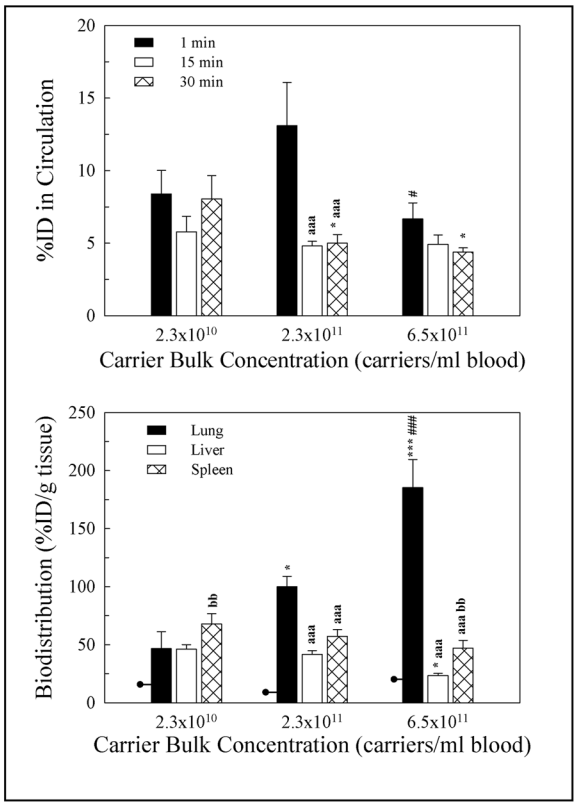

Figure 2. Effects of bulk concentration of anti-ICAM carriers on endothelial targeting in mice

(A) Circulation at 1 min, 15 min, and 30 min of ^{125}I-labeled anti-ICAM carriers (6,650 Ab/μm^2) injected i.v. in anesthetized C57Bl/6 mice at varying carrier concentrations (as indicated), expressed as the percentage of the injected dose (%ID). (B) Biodistribution of said carriers at 30 min after injection, calculated as % ID per gram of organ. Data are mean ± SEM (n ≥ 3 mice). Lines intersecting lung bars are levels for IgG carriers. Among different groups of carriers: * compares each carrier concentration to carriers = 2.3 × 1010 carriers/ml blood; # compares carriers at 6.5 × 1011 carriers/ml blood to carriers at 2.3 × 1011 carriers/ml blood. Within the same group of carrier: a compares each time to 1 min; b compares 30 min to 15 min. *, #, a, and b are $p \leq 0.05$; **, ##, aa, and bb are $p \leq 0.01$; ***, ###, aaa, and bbb are $p \leq 0.001$, by Student's *t*-test.

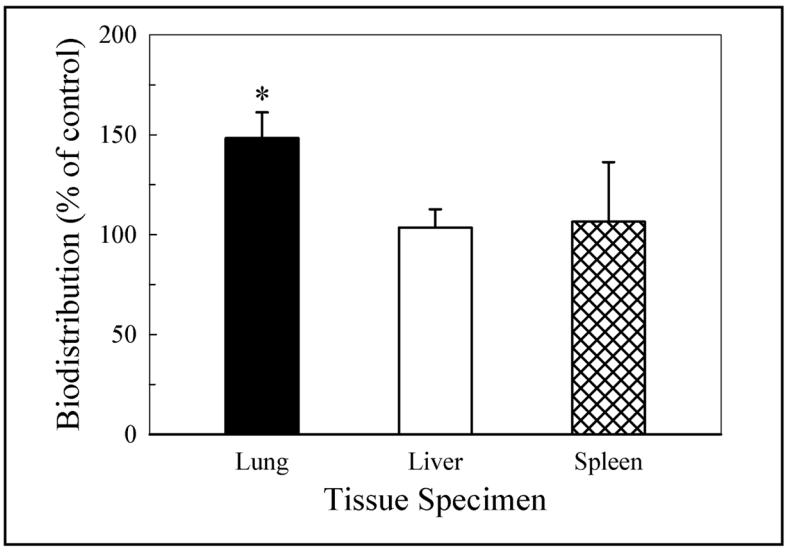

Figure 3. Effects of LPS on endothelial targeting of anti-ICAM carriers in mice

Biodistribution of 125I-labeled anti-ICAM carriers (23×10^{10} carriers/ml blood, 6,650 Ab/μm^2) at 30 min after injection in anesthetized C57Bl/6 mice (control or pre-treated for 16 h with LPS), calculated as % ID per gram of organ. LPS data are normalized to results in control mice. Data are mean ± SEM (n ≥ 3 mice). * compares LPS to control; $p \leq 0.05$, by Student's *t*-test.

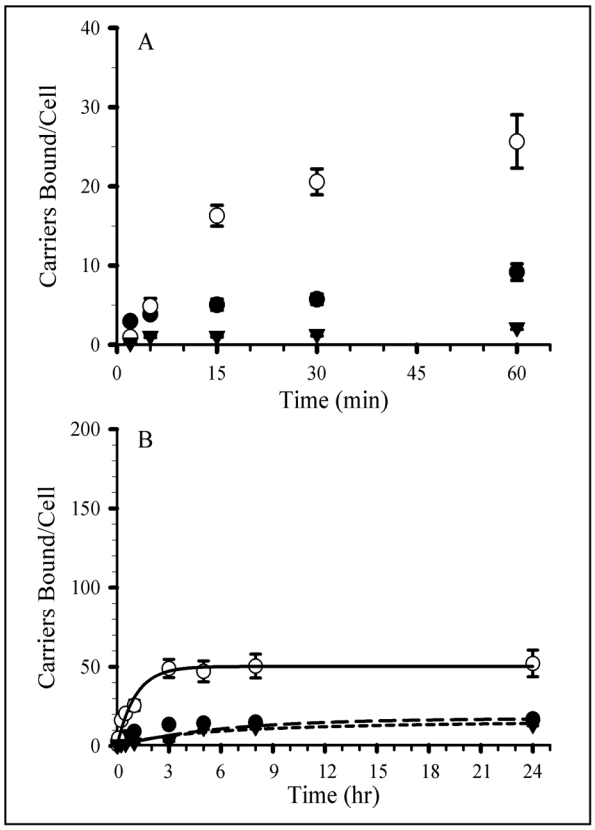

Figure 4. Effects of Ab-surface density of anti-ICAM carriers on targeting to quiescent endothelial cells

Two anti-ICAM carrier densities (1,100 and 4,100 Ab/μm^2) were targeted to fixed, non-activated HUVEC. (A) Kinetics of binding from 0 to 60 min. (B) Kinetics of binding from 0 to 24 hr. Symbols are: open circles, 4,100 Ab/μm^2 anti-ICAM carriers; closed circles, 1,100 Ab/μm^2 anti-ICAM carriers; closed triangles, 4,100 Ab/μm^2 IgG carriers. Error bars correspond to SEM; some error bars are smaller than the symbol size shown. Regression lines were calculated using SigmaPlot.

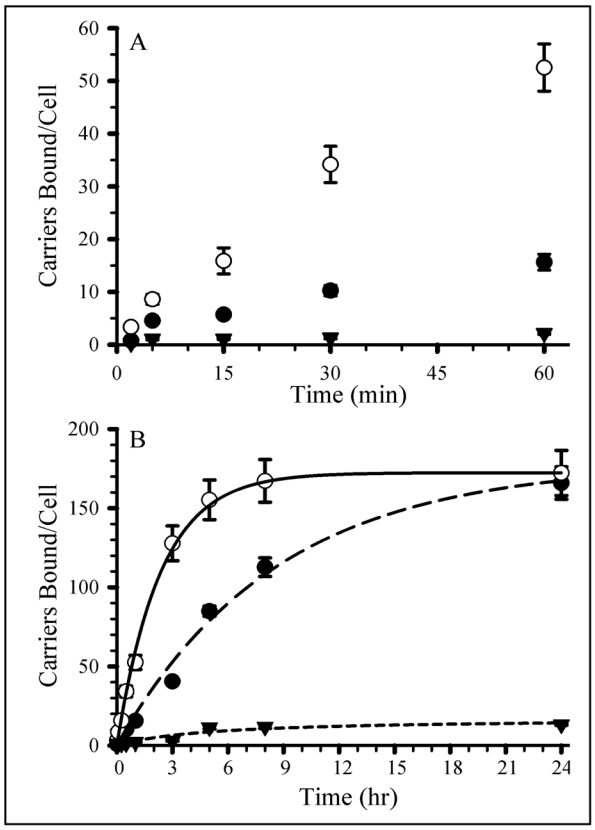

Figure 5. Effects of Ab-surface density of anti-ICAM carriers on targeting to activated endothelial cells

Two anti-ICAM carrier densities (1,100 and 4,100 Ab/μm^2) were targeted to fixed, TNF-α activated HUVEC. (A) Kinetics of binding from 0 to 60 min. (B) Kinetics of binding from 0 to 24 hr. Symbols are: open circles, 4,100 Ab/μm^2 anti-ICAM carriers; closed circles, 1,100 Ab/μm^2 anti-ICAM carriers; closed triangles, 4,100 Ab/μm^2 IgG carriers. Error bars correspond to SEM; some error bars are smaller than the symbol size shown. Regression lines were calculated using SigmaPlot.

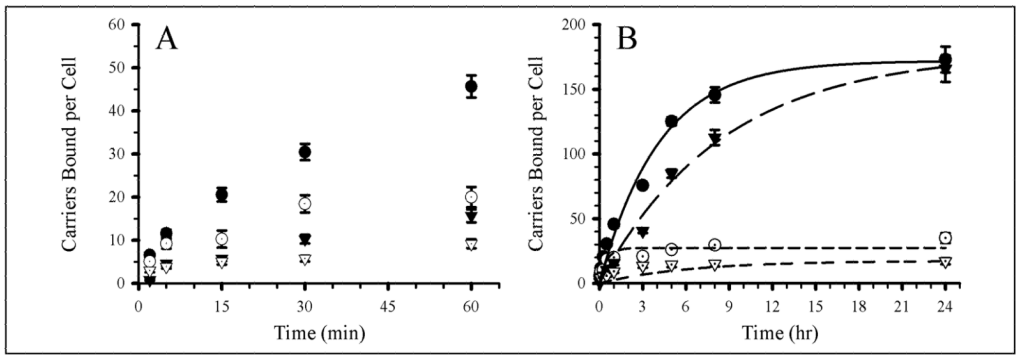

Figure 6. Effects of anti-ICAM carrier concentration with low Ab-surface density on targeting to quiescent vs activated endothelial cells

Anti-ICAM carriers bearing 1,100 Ab/μm^2 were targeted to fixed, quiescent vs TNF-α activated HUVEC at two carrier concentrations (6.8 × 10^8 and 13 × 10^8 carriers/ml cell media). (A) Kinetics of binding from 0 to 60 min. (B) Kinetics of binding from 0 to 24 hrs. Open symbols refer to quiescent cells and closed symbols refer to activated cells. Circles are used for high concentration (13 × 10^8 carriers/ml media) conditions and triangles are used for low concentration (6.8 × 10^8 carriers/ml media) conditions. Error bars correspond to SEM; some error bars are smaller than the symbol size shown. Regression lines were calculated using SigmaPlot.

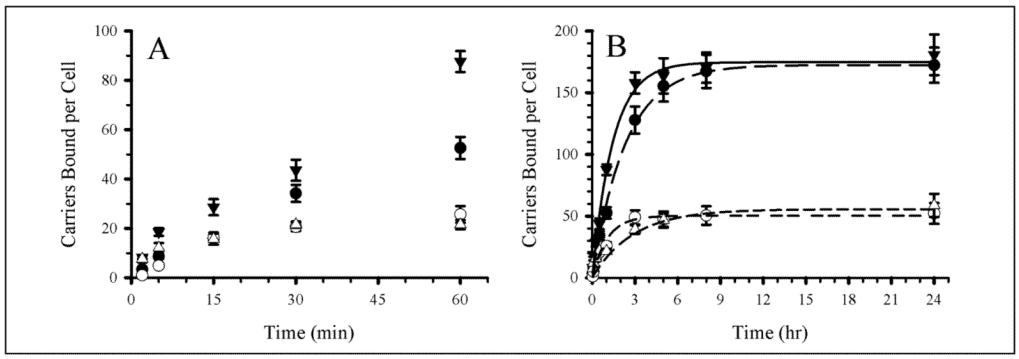

Figure 7. Effects of anti-ICAM carrier concentration with high Ab-surface density on targeting to quiescent vs activated endothelial cells

Anti-ICAM carriers bearing 4,100 Ab/μm^2 were targeted to fixed, quiescent vs TNF-α activated HUVEC at two carrier concentrations (6.8×10^8 and 13×10^8 carriers/ml cell media). (A) Kinetics of binding from 0 to 60 min. (B) Kinetics of binding from 0 to 24 hrs. Open symbols refer to quiescent cells and closed symbols refer to activated cells. Circles are used for high concentration (13×10^8 carriers/ml media) conditions and triangles are used for low concentration (6.8×10^8 carriers/ml media) conditions. Error bars correspond to SEM; some error bars are smaller than the symbol size shown. Regression lines were calculated using SigmaPlot

Table 1
Parameters of anti-ICAM carriers tested in vivo

(Carrier size: 179 ± 38 nm)

Carrier Surface Area Density μm^2/ml blood	Carrier Bulk Concentration carriers/ml blood	Ab Surface Concentration molecules/μm^2	Ab Concentration molecules/carrier	Ab Bulk Density molecules/ml blood
7.2×10^8	2.3×10^{10}	6,650	209	48×10^{11}
72.2×10^8	23×10^{10}	0	0	0
72.2×10^8	23×10^{10}	1,750	55	126×10^{11}
72.2×10^8	23×10^{10}	5,250	165	379×10^{11}
72.2×10^8	23×10^{10}	6,650	209	481×10^{11}
72.2×10^8	23×10^{10}	6,935	218	501×10^{11}
204.1×10^8	65×10^{10}	6,650	209	$1,357 \times 10^{11}$

Control IgG carriers are represented as 0 Ab/μm^2

Table 2
Parameters of anti-ICAM carriers tested in cell cultures

(Carrier size: 1.14 ± 0.21 μm)

Carrier Surface Area Density μm^2/ml cell media	Carrier Bulk Concentration carriers/ml cell media	Ab Surface Concentration molecules/μm^2	Ab Concentration molecules/carrier	Ab Bulk Density molecules/ml cell media
21.3×10^8	6.8×10^8	1,100	3,460	23.4×10^{11}
21.3×10^8 [a]	6.8×10^8 [a]	4,100 [a]	12,900 [a]	87.3×10^{11} [a]
40.8×10^8	13×10^8	1,100	3,460	44.9×10^{11}
40.8×10^8	13×10^8	4,100	12,900	167.4×10^{11}

[a] Condition at which control IgG carriers were compared to anti-ICAM carriers

Table 3

In vivo endothelial targeting of anti-ICAM carriers as a function of the Ab dose injected.

Ab Bulk Density molecules/ml blood	%ID/g Lung	%ID/g Liver	%ID/g Spleen
0	9.3 ± 1.4	51 ± 3.6	98.9 ± 7.8
48×10^{11}	46.7 ± 14.5	46.2 ± 3.6	67.9 ± 8.7
126×10^{11}	55.8 ± 6.7	47.6 ± 0.7	72.9 ± 3.1
379×10^{11}	62.7 ± 5.9	46.2 ± 3.9	66.7 ± 12.0
481×10^{11}	99.9 ± 9.0	41.6 ± 3.9	57.3 ± 5.7
501×10^{11}	125.0 ± 16.8	45.0 ± 6.2	65.4 ± 7.0
$1{,}357 \times 10^{11}$	185.3 ± 24.3	23.4 ± 1.8	47.1 ± 6.7

Control IgG carriers are represented as 0 Ab/μm^2; Data are presented using mean ± SEM (n ≥ 3 mice).

Table 4

In vitro endothelial targeting of 1 μm anti-ICAM carriers.

Experimental Conditions and Parameters	Experimental Half Time $t_{1/2}$ (min)	Experimental B_{sat} (Particles/Cell)	Theoretical Half Time K_t (min)
4,100 Ab/μm^2, TNF−, LC	60	52 ± 8.4	63.7
1,100 Ab/μm^2, TNF−, LC	250	16±2.7	370.4
4,100 Ab/μm^2, TNF−,HC	60	58±9.4	172.4
1,100 Ab/μm^2, TNF−, HC	30	35±3.9	29.8
4,100 Ab/μm^2, TNF+, LC	120	171±14.0	140.8
1,100 Ab/μm^2, TNF+, LC	300	165±10.2	555.6
4,100 Ab/μm^2, TNF+, HC	60	180±16.5	87.7
1,100 Ab/μm^2, TNF+, HC	180	173±10.8	250.0

Parameter $t_{1/2}$ was an experimental halftime of saturation; the parameter K_t was a theoretical halftime calculated from regressions using SigmaPlot. LC and HC correspond to low and high concentrations 6.8×10^8 and 13×10^8 carriers/ml cell media, respectively. Data are presented using mean ± SEM ($n \geq 25$).

Table 5

Avidity parameters of 1 μm carriers to in vitro endothelial cells.

Activation State	1,100 Ab/mm^2		4,100 Ab/mm^2	
	K_d (pM)	B_{max}	K_d (pM)	B_{max}
TNF (−)	8.6	44	5.9	55
TNF (+)	2.9	170	1.6	175

Values of K_d and B_{max} were calculated from Scatchard plots using anti-ICAM carriers targeted to HUVEC cells.